Published in final edited form as:
Mol Biosyst. 2010 September ; 6(9): 1640–1649. doi:10.1039/c001975e.

Using a genetically targeted sensor to investigate the role of presenilin-1 in ER Ca^{2+} levels and dynamics

Janet E. McCombs[1], **Emily A. Gibson**[2], and **Amy E. Palmer**[1,*]

[1] UCB 215, Department of Chemistry and Biochemistry, University of Colorado, Boulder, CO 80309

Summary

The ER plays a fundamental role in storing cellular Ca^{2+}, generating Ca^{2+} signals, and modulating Ca^{2+} in both the cytosol and mitochondria. Genetically encoded Ca^{2+} sensors can be explicitly targeted to the ER to directly define Ca^{2+} levels and monitor fluxes of Ca^{2+} within this organelle. In this study we use an ER-targeted Ca^{2+} sensor to define both the level and dynamics of ER Ca^{2+} in cells expressing mutant presenilin proteins. Growing evidence suggests the enigmatic presenilin-1 plays a role in regulating ER Ca^{2+}. Presenilin-1 was initially identified in a screen for genetic causes of inherited familial Alzheimer's disease (fAD). The connection between presenilin-1, calcium regulation, and Alzheimer's disease may provide the key to understanding the long-observed, but poorly understood, link between Alzheimer's disease and Ca^{2+} dysregulation. In this study we examined seven fAD-causing mutations in presenilin-1 to define how they influence ER Ca^{2+} levels and dynamics. We observed that some, but not all, mutations in PS1 decrease the level of Ca^{2+} within the ER and this difference depends on the enzymatic activity of PS1. Two mutations tested altered the kinetics of Ca^{2+} release from the ER upon ATP stimulation, resulting in faster spiking. Combined, these results indicate that mutations in PS1 can alter the balance of Ca^{2+} in cells and have the potential to influence the nature of Ca^{2+} signals.

Introduction

Ca^{2+} is an essential and tightly regulated cellular second messenger, important for the maintenance of many cellular processes and functions. Ca^{2+} signals can be generated by influx across the plasma membrane or release of Ca^{2+} from the Endoplasmic Reticulum (ER), which serves as the storehouse and signaling hub of Ca^{2+}. Recently, presenilin-1 (PS1) has emerged as a central player in the regulation of ER Ca^{2+}[1-3]. An integral membrane protein predominantly localized to the ER, PS1 has been proposed to: form a Ca^{2+} leak channel in the ER [1]; interact with and regulate the Sarco/endoplasmic reticulum Ca^{2+} ATPase (SERCA) [2]; modulate release of Ca^{2+} through the IP_3 receptor (IP_3R) [3]; and interact with, change the expression levels of, and modify Ca^{2+} release through the Ryanodine Receptor (RyR) [4, 5].

PS1 was originally identified in a genetic screen for causative agents of familial Alzheimer's disease (fAD) [6]. Since then, over 150 mutations in PS1 have been identified that give rise to fAD. The involvement of PS1 in Alzheimer's disease pathology has been primarily ascribed

* to whom correspondence should be addressed: amy.palmer@colorado.edu, 303-492-1945.
[2]current address: Department of Physics, University of Colorado, Denver, CO 80217

Online supplemental materials
The following supplemental materials are available online: Supplementary Methods, Supplementary Figure S1: Demonstration of γ-secretase activity in MEF cells, Supplementary Figure S2: The effect of PS1 on ATP-induced ER Ca^{2+} release, and Supplementary Figure S3: Analysis of calcium spiking data using IGOR Pro.

to altered processing of the amyloid precursor protein (APP) by gamma-secretase, a multi-protein complex containing PS1 [7]. Both sporadic and inherited cases of Alzheimer's disease are characterized by Ca^{2+} imbalance and growing evidence indicates that Ca^{2+} dysregulation is correlated with disease pathogenesis [8-10]. To assess whether the Ca^{2+}-regulatory function of PS1 is relevant to fAD, it is important to define how mutations in PS1 alter these functions. Though its exact role is unclear, mutations in PS1 have been suggested to cause both overloading and under-filling of ER Ca^{2+} stores, and to both increase and decrease Ca^{2+} release from the ER [1, 3, 11-15].

Due to the complexity of cellular Ca^{2+} regulation, live cell imaging of Ca^{2+} signaling events are greatly benefited by sensors targeted to specific subcellular compartments. However, many studies investigating the role of PS1 mutations on Ca^{2+} dyshomeostasis have inferred the impact on ER Ca^{2+} by measuring changes in cytosolic Ca^{2+}. Such studies may be confounded by changes in cytosolic clearance mechanisms and discrepancies between ER Ca^{2+} load and Ca^{2+} release. Genetically encoded Ca^{2+} sensors, such as cameleons, can be specifically targeted to the ER, permitting investigators to monitor Ca^{2+} within the ER (i.e. ER Ca^{2+} load), directly observe the leak or release of Ca^{2+} from this organelle, and examine SERCA activity by measuring Ca^{2+} uptake. Despite these advantages, these sensors have remained underutilized tools in studies examining effects of disease on cellular Ca^{2+} homeostasis. In the present study, we apply one such sensor, D1ER [16], and examine a panel of fAD-associated mutations in PS1 to determine their effects on ER Ca^{2+} levels and dynamics. We found that mutations in PS1 indeed alter ER Ca^{2+}, but not all mutations have the same effect. Alteration of ER Ca^{2+} levels by mutant PS1 could be reversed by addition of a gamma secretase inhibitor, suggesting that PS1 enzymatic activity impacts ER Ca^{2+} levels. In addition, because ER Ca^{2+} release can impact downstream signaling processes, we examined whether mutations in PS1 affected Ca^{2+} release from the ER upon stimulation with ATP. Two mutants tested led to an increase in the frequency of Ca^{2+} spikes, suggesting that mutations in PS1 affect the nature of ER Ca^{2+} release.

Results

To examine whether mutations in PS1 affect Ca^{2+} in a universal manner we chose a range of mutations localized throughout PS1 that vary in their average age of Alzheimer's disease onset (Figure 1A). Mouse embryonic fibroblast (MEF) cells deficient in PS1 and PS2 (double knock out, DKO) were used as a model to eliminate potential effects of endogenous PS on the Ca^{2+} phenotype [17, 18]. DKO MEF cells were reconstituted with WT or mutant PS1 by transient transfection and the presence of PS1 in cells was confirmed by GFP or mCherry fluorescence. Reconstitution of PS1 was corroborated by Western blot (Figure 1B).

Mutations in PS1 have differential effects on ER Ca^{2+} store levels

The amount of Ca^{2+} within the ER is a balance of the ER buffering capacity, activity of the SERCA pump, release through channels and a passive “leak” of Ca^{2+} out of the ER. For this study, steady state levels of ER Ca^{2+} were determined by measuring the resting FRET ratio (R) using the D1ER cameleon sensor. Subsequent inhibition of SERCA with thapsigargin led to a decrease in R as Ca^{2+} slowly leaks out of the ER (Figure 2A), enabling us to determine relative ER Ca^{2+} levels. Under resting conditions, DKO cells exhibited a higher normalized ratio (ΔR), indicative of higher $[Ca^{2+}]_{ER}$ when compared to WT and DKO cells reconstituted with WT PS1 (referred to as DKO + WT, Figure 2B). This is consistent with previous studies using these MEF cells in which the low affinity Ca^{2+} sensor MagFura-2 was used to measure $[Ca^{2+}]_{ER}$ [1, 12].

Figure 2B also presents results for the PS1 variants examined in this study, illustrating that different mutants have differential effects on ER Ca^{2+} stores. WT cells consistently yielded

a Ca^{2+} phenotype that was the same as DKO + WT. For statistical analysis, all mutant PS1 were compared to DKO + WT, allowing direct comparison of the impact of a specific mutation on Ca^{2+} within the same genetic background. Compared to DKO + WT, only M233V and A409T showed a statistically significant decrease in $[Ca^{2+}]_{ER}$ ($P < 0.05$, ANOVA). V94M appeared to have a slightly increased Ca^{2+} level compared to reconstituted cells; however, this difference was not statistically significant. Our data support a role for PS1 in regulation of ER Ca^{2+} levels, though it is clear that not all mutations in PS1 affect the Ca^{2+} level within the ER.

Green, *et al.*, recently proposed that PS1 regulates SERCA pump activity [2]. Since SERCA is responsible for pumping Ca^{2+} into the ER, an over- or under-active SERCA could result in over- or under-filling of the ER store. To examine SERCA pump activity, cells were treated with the reversible SERCA inhibitor tBHQ leading to depletion of ER Ca^{2+}. Once ER Ca^{2+} levels stabilized, tBHQ was washed out and Ca^{2+} added back, causing an influx of Ca^{2+} into internal stores through the SERCA pump. D1ER enabled us to directly monitor changes in $[Ca^{2+}]_{ER}$ as shown in Figure 2C. The rate constant for re-filling was found by fitting the Ca^{2+} influx curve to a single exponential rise (Figure 2D), and was significantly higher in WT as compared to DKO cells ($k_{WT} = 15.0 \times 10^{-3} \pm 1.2 \times 10^{-3}$ s^{-1}, $k_{DKO} = 8.1 \times 10^{-3} \pm 2.2 \times 10^{-3}$ s^{-1}, $P < 0.015$, ANOVA), consistent with previous findings suggesting PS1 increases SERCA pump activity [2]. To examine whether mutations in PS1 affect this regulatory function, we focused on PS1 variants that led to a detectable change in ER Ca^{2+} levels. However, we found that none of the mutants tested had an effect on Ca^{2+} influx through SERCA (Figure 2E), indicating that although PS1 impacts SERCA pump activity, the mutations in PS1 examined here do not appear to affect this function. Interestingly, the differences in the ER Ca^{2+} load can not be explained by SERCA activity alone, as cells containing WT PS1 had greater SERCA activity, but overall lower Ca^{2+} when compared to DKO.

In addition to regulating ER Ca^{2+} stores, previous studies have suggested PS1 forms a leak channel in the ER [1] or contributes to the rate at which Ca^{2+} leaks out of the ER [3]. To examine the leak rate, the change in R within the ER was monitored upon inhibition of SERCA with thapsigargin. Figure 3 presents the initial rate of decay (linear fit to the first 150 s of the R curve upon thapsigargin treatment) and the rate of change as a function of the Ca^{2+} level ($d\Delta R/dt$). Because PS mutations differentially affect the level of Ca^{2+} in the ER (Figure 2B), we felt it was important to compare the leak rate as a function of Ca^{2+} to ensure that any potential differences in leak rate were not simply reflections of the different amount of Ca^{2+} at a given point in time. No difference in Ca^{2+} leak rate was observed between DKO and WT cells (Figure 3A and 3B); however, three of the mutants tested exhibited an altered leak rate compared to WT cells. V94M exhibited a greater leak for both the initial rate and the leak rate as a function of ER Ca^{2+} level, while M233V and A409T both exhibited a lower leak (Figure 3). These results indicate that mutations in PS1 can affect the rate at which Ca^{2+} leaks out of the ER, with some mutations causing an increase in the leak and some causing a decrease. However, it is clear that the ER Ca^{2+} load is not defined by the leak rate, but rather the altered leak rate may be a consequence of altered Ca^{2+} load as mutations that cause a decrease in the ER Ca^{2+} load yield a lower leak rate, and vice versa.

ER levels are regulated by PS1 activity

In addition to its Ca^{2+} regulatory functions, PS1 serves as the catalytic subunit of the multi-protein gamma-secretase complex, which cleaves a number of substrates in the cell, including APP. APP is a single pass transmembrane protein that is cleaved by gamma-secretase into two fragments: an intracellular domain and an extracellular peptide called amyloid beta (Aβ). The activity of our PS1 mutants within the gamma-secretase complex was verified using an APP-C99-mCherry probe to show cleavage of APP in cells

(Supplementary Figure S1). As altered ER Ca^{2+} levels could not be explained by SERCA activity or the leak rate of Ca^{2+} out of the ER, we next examined whether the activity of PS1 as part of the gamma-secretase complex affected ER Ca^{2+} homeostasis by using the small molecule gamma-secretase inhibitor N-[N-(3,5-Difluorophenacetyl-L-alanyl)]-S-phenylglycine *t*-Butyl Ester (DAPT). Treatment with DAPT had no effect on $[Ca^{2+}]_{ER}$ in DKO + WT, V94M, and L166P cells. However, inhibition of gamma-secretase activity resulted in an enhancement of ER Ca^{2+} levels for both M233V and A409T, raising them to DKO + WT levels (Figure 4A). Moreover the leak rates for all mutants examined were comparable to WT, consistent with leak rate being a consequence of the ER Ca^{2+} load (Figure 4B – D). To assess whether changes in Ca^{2+} could be attributed to the gamma-secretase mediated cleavage products of APP, the relative amounts of two cleavage products (Aβ40 and Aβ42) were determined by ELISA (Figure 5). While the observed changes in Aβ cleavage products are intriguing and may have implications for Alzheimer's disease progression (L166P and M233V have the highest Aβ42/40 ratios and the earliest ages of onset in 24 and 32 yrs, respectively), these changes do not correlate with changes in ER Ca^{2+}. For example, M233V and A409T are the two mutants with reduced ER Ca^{2+} and inhibition of gamma secretase increases Ca^{2+} to WT levels. However these two mutants have very different Aβ profiles. Therefore while gamma secretase activity plays a role in influencing ER Ca^{2+} levels, this can not be easily ascribed to Aβ cleavage products. Overall our data reveal that there may be multiple mechanisms by which PS1 affects ER Ca^{2+} levels, one dependent on and another independent of gamma secretase activity. Comparison of DKO and DKO + WT reveals that PS1 lowers ER Ca^{2+} levels regardless of its enzymatic activity. This is confirmed by measurement of the ER Ca^{2+} load in DKO cells expressing a catalytically inactive PS1 mutant (D257A) which phenocopies the DAPT-inhibited DKO + WT cells. However AD-causing mutations in PS1 can lead to additional alterations in ER Ca^{2+} (i.e. a further decrease for M233V and A409T compared to WT PS1), and this additional perturbation is clearly dependent on gamma secretase activity as the difference could be reversed by DAPT inhibition.

Mutations in PS1 affect the kinetics of ER Ca^{2+} release

As the central storehouse of Ca^{2+} the ER plays a central role in generation of Ca^{2+} signals. For example activation of P2Y G-protein coupled receptors by ATP leads to the production of IP_3 and release of Ca^{2+} from the ER. Repetitive release leads to the generation of Ca^{2+} oscillations in the cytosol, the duration, amplitude and frequency of which affect downstream processes such as cell cycle regulation, gene transcription, and differentiation [19]. A recent report indicates that PS1 interacts with the IP_3R to modulate the open probability and hence release of Ca^{2+} from the ER [3]. Moreover, an fAD-associated mutation (M146L) was shown to alter release of Ca^{2+} through the IP_3R independent of Ca^{2+} load. For this study, we chose to examine the L166P, M233V, and A409T mutants as they showed a change in Aβ production and/or lowered $[Ca^{2+}]_{ER}$ levels. Cells stimulated with 5 μM ATP exhibited two categories of response: immediate response with rapid Ca^{2+} spiking followed by slower irregular transients or a delayed response with no repetitive Ca^{2+} fluctuations. Investigation into the nature of ATP-induced Ca^{2+} release resulted in no observable difference in ATP sensitivity for L166P and A409T, but a decrease in sensitivity (as defined by decreased responsiveness to ATP) for M233V (Supplementary Figure S2A and B). A general decrease in the amplitude of Ca^{2+} release was observed for L166P and M233V, but not A409T, even though it contains less Ca^{2+} in the ER than WT (Supplementary Figure S2C – H).

Given the versatility of Ca^{2+} signaling, cells can interpret changes in frequency of Ca^{2+} oscillations in order to differentially control multiple cellular processes [19]. Because of this, changes in the kinetics of Ca^{2+} release through the IP_3R could alter the fate of a cell,

contributing to a diseased state. We therefore examined how the mutations studied here affected the frequency of the ATP-induced Ca^{2+} signals. Treatment of cells with 5 μM ATP lead to a rapid burst of Ca^{2+} spikes superimposed on a broad Ca^{2+} decay curve (Figure 6A left side). Longer imaging revealed irregular slower Ca^{2+} transients in a small subset of cells (Figure 6A right side). Attempts to elicit more regular extended oscillations in a larger fraction of cells using different stimuli (ATP, UTP, histamine, and carbachol) and lower doses of stimuli (i.e. 1 μM ATP vs. 5 μM ATP) were unsuccessful. Therefore we focused our analysis on the rapid initial bursting of Ca^{2+}, as this bursting is still dependent on release from the IP_3R and allows comparison of the kinetics of release between the different mutants. Figure 6 shows representative traces which reveal that cells expressing M233V and A409T, but not L166P, exhibited faster spiking than either WT or DKO cells. In an attempt to quantify the differences between cells expressing mutant PS1, we calculated the spike period (i.e. time between spikes from peak to peak) for every cell that exhibited repetitive spiking (see experimental section). These data are presented in the histograms (Figure 6, right side) which show that cells expressing M233V or A409T exhibit a greater percentage of faster spike periods (histogram shifted to lower time intervals). Given that many downstream effectors of Ca^{2+} signaling "read-out" both the amplitude and frequency of the Ca^{2+} signal, the fact that mutations in PS1 can alter the kinetics of ER Ca^{2+} release may play a significant role in eliciting Ca^{2+} dyshomeostasis.

Discussion

Calcium homeostasis is tightly regulated by dynamic interplay between channels, pumps, and transporters that control Ca^{2+} levels in the ER, mitochondria, and cytosol. Genetically targeted sensors provide a powerful way of monitoring Ca^{2+} directly within each of these locales. This feature may be especially important because cells appear to be adept at compensating for perturbations to Ca^{2+} homeostatic mechanisms. If a perturbation, such as expression of mutant presenilin-1, alters Ca^{2+} homeostasis the cell may compensate to minimize the perturbation, such as upregulating or downregulating channels or pumps. Indeed, in this study we found that the ER Ca^{2+} leak is altered by changes in ER Ca^{2+} levels such that lower ER Ca^{2+} levels lead to a decreased leak rate. This compensation is dynamic and could be reversed by elevating ER Ca^{2+} levels using DAPT. These results reinforce the importance of directly measuring $[Ca^{2+}]_{ER}$ to investigate ER Ca^{2+} homeostasis, as measurement of cytosolic Ca^{2+} to interpret ER load may be confounded by compensatory changes in channels and pumps that exist to maintain cytosolic Ca^{2+}.

Deletion of PS1 caused a significant increase in ER Ca^{2+}, consistent with some, but not all studies which have measured Ca^{2+} directly within the ER. There are three methods for measuring Ca^{2+} within the ER: the D1ER sensor employed in this study, the low affinity Ca^{2+} indicator MagFura-2, and an ER-targeted aequorin-based sensor. It should be noted that a fourth method has been used to indirectly infer the ER Ca^{2+} load by measuring how much Ca^{2+} is released into the cytosol upon treatment with the ionophore ionomycin [1, 12]. This approach suffers from two drawbacks: it measures release from all internal compartments, not just the ER, and it cannot account for potential differences in cytosolic clearance mechanisms that may arise if Ca^{2+} homeostasis is perturbed. Given that PS1 alters many aspects of Ca^{2+} homeostasis, we suspect direct measurement of ER Ca^{2+} is likely to be a more accurate measure of the ER Ca^{2+} load and for this, D1ER possesses some advantages. First, both MagFura-2 and aequorin require additional cellular manipulation for loading the sensors into internal compartments. MagFura-2 relies on permeabilization, ER store depletion, and addition of MgATP to activate store refilling, while aequorin requires ER store depletion, reconstitution of cells with coelenterazine, and store re-filling upon addition of extracellular Ca^{2+}. Second, both of these approaches infer resting Ca^{2+} levels by monitoring store re-filling after depletion, which may be complicated by differences in

SERCA pump activity. For example, in a study using MagFura-2, Cheung et al. found that untransfected DT40 cells filled to a higher level than cells transfected with PS1, consistent with our findings for DKO vs. WT cells [3]. However, two studies using ER-targeted aequorin found that PS1 deficient cells filled to a lower level than cells containing PS1 [13, 20]. These experiments inadvertently rely on SERCA activity for measuring ER load, and one interpretation of the reported discrepancies is that different conditions for re-loading intracellular stores may promote differential re-filling of the ER.

By using the genetically encoded Ca^{2+} sensor D1ER, we were able to directly monitor ER Ca^{2+} levels and dynamics, including leak rates of Ca^{2+} out of the ER and uptake into the ER. We discovered that fAD-associated mutations in PS1 differentially affect levels of Ca^{2+} in the ER and leak from the ER. This helps put into context the numerous, but often conflicting studies that have examined individual mutations in PS1. Here we found one mutation that appeared to increase both ER Ca^{2+} and the leak rate (V94) and two that decreased ER Ca^{2+} and the leak rate (M233V and A409T). However, a number of mutations had no effect on ER Ca^{2+} levels, further suggesting that there is not a universal phenotype for perturbation of ER Ca^{2+} by mutant PS1. Unfortunately, the mechanism(s) by which PS1 mutations alter ER Ca^{2+} levels remain enigmatic. In particular, changes in the leak rate appeared to be a consequence rather than a cause of altered ER Ca^{2+}. Likewise, PS1 increases SERCA activity, but leads to a decrease in ER Ca^{2+} load. Intriguingly, inhibition of the proteolytic activity of PS1 (as part of the gamma secretase complex) affected cells expressing mutant PS1 but not WT PS1 strongly suggesting there are multiple mechanisms by which PS1 can influence ER Ca^{2+}. Combined, these factors (compensatory changes and the possibility of multiple mechanisms) make it difficult for us to define the molecular mechanism by which f-AD causing mutations in PS1 alter ER Ca^{2+}, and thus these mechanism(s) remain elusive. On the other hand, our results do help provide a framework for understanding the sometimes conflicting studies on PS1 and fAD-causing mutations. In particular, they highlight that different mutations in PS1 give rise to different Ca^{2+} phenotypes and that many aspects of Ca^{2+} regulation may be altered in mutant PS1 cells, some of which are compensatory changes that result from PS1 expression.

The two mutations that lead to a significant decrease in ER Ca^{2+} (M233V and A409T) also gave rise to altered kinetics of Ca^{2+} release from the ER upon ATP stimulation, exhibiting an increase in the frequency of Ca^{2+} bursting. To our knowledge, M146L is the only other PS1 mutation examined for its ability to influence release kinetics. Cheung et al[3] found that M146L lead to enhanced Ca^{2+} oscillation frequency and this was due to altered gating of the IP_3R. Interestingly, this mutant also gave rise to a lower ER Ca^{2+} load. Our results are consistent with this finding, further supporting the notion that PS1 interacts with and modulates the IP_3R. Given that release of Ca^{2+} from the ER results in signals that are decoded by the cell to control cellular function, an important next step will be to identify the consequences of these altered signals and what role, if any, these changes play in Alzheimer's disease. A growing body of evidence including the results presented here, indicate that in addition to modulating ER Ca^{2+} levels, fAD-causing mutations in PS1 contribute to an overall dysregulation of Ca^{2+}, including alteration of fundamental Ca^{2+} signals.

In summary, our study demonstrates the power of an ER-targeted Ca^{2+} sensor by illustrating that the sensor can be used to directly monitor Ca^{2+} levels, Ca^{2+} leak from the ER, and uptake into the ER. Overall, we show that mutations in PS1 give rise to numerous and varied changes in Ca^{2+} which we hope will provide a framework for interpreting reports on ER Ca^{2+} in AD as well as other diseases.

Experimental

Cell culture and transfections

Wild type (WT) and presenilin-1/2- double knock out (DKO) mouse embryonic fibroblasts (MEFs) were obtained from Dr. Bart de Strooper, Katholieke Universiteit Leuven, Leuven, Netherlands [17, 18] and were cultured in DMEM supplemented with 10% (v/v) FBS and 1% (v/v) penicillin and streptomycin. Due to the propensity for MEFs to accumulate mutations over time, cells were only used through passage number 20. DKO cells were reconstituted with either mutant or WT PS1 by transient transfection using TransIT (Mirus), and the resulting Ca^{2+}-phenotype was compared to WT MEF cells. Cells were imaged 24-48 h post-transfection.

Cloning and constructs

For PS1 constructs, the I-467 isomer of human PS1 (NM_000021) was purchased from OriGene Technologies, Inc. AD-causing mutations were generated using QuikChange® Site-Directed Mutagenesis (Stratagene). PS1 variants were cloned into pRex-IRES-GFP and pRex-IRES-mCherry vectors (Dr. Xuedong Liu, University of Colorado-Boulder) between BamHI and NotI sites. These vectors encode an internal ribosomal entry site between the PS1 and fluorescent protein gene, enabling the selection of PS1-expressing cells on the basis of fluorescence.

Western blotting

Cells transfected with mutant PS1 in the pRex-IRES-GFP vector were washed in ice-cold Phosphate Buffered Saline (PBS) before being scraped into 1 mL PBS and spun down at 3000 *g* for 5 minutes. To lyse cells, pellets were re-suspended in STEN buffer (50mM Tris-HCl, pH 7.6, 150mM NaCl, 2mM EDTA, 1% TritonX-100 and 0.2% NP-40, plus protease inhibitor cocktail) and incubated on ice for 30 minutes. Lysis suspensions were spun down at 21000 *g* for 20 minutes to remove cell debris. Total protein concentration was determined using the BCA Protein Assay kit (Pierce) prior to separation on a 4 - 20% Tris-HEPES-SDS polyacrylimide gel and transfer to a PVDF membrane. Membranes were blocked in Tris-buffered saline supplemented with 0.1% (v/v) Tween-20 (TBS-T) and 5% (w/v) milk for 1 h at room temperature. To probe membranes, we used the anti-PS1 antibody APS18 (3μg/mL; Novus Biologicals) and anti-β-actin antibody (1:5000; Sigma). Proteins were detected by incubating in a Rabbit anti-mouse HRP conjugated secondary antibody (Zymed). Although we attempted numerous times, we could not get the APS18 antibody to detect the endogenous mouse PS1 in MEF cells. Therefore we cannot directly compare the level of human PS1 in reconstituted cells, to endogenous levels of mouse PS1.

Instrumentation for fluorescence microscopy

For imaging experiments, cells were washed and placed in Hank's Balanced Salt Solution with HEPES (20mM HEPES, 1X HBSS (Gibco), and 2g/L D-glucose, pH 7.2) or Ca^{2+}-free HHBSS (20mM HEPES, 1X HBSS without Ca^{2+}, Mg^{2+}, or sodium bicarbonate, 2g/L D-glucose, 490μM $MgCl_2$, 450μM $MgSO_4$, pH 7.2). Imaging experiments were conducted at room temperature (25 °C). Fluorescence imaging was performed on an Axiovert 200M wide-field microscope (Zeiss) equipped with a Lambda 10-3 filter changer (Sutter Instruments) and Cascade 512B camera (Photometrics) for rapid acquisition of ratio images. Images were acquired using METAFLUOR software (Universal Imaging). All experiments were performed using a 1.3 NA 40X objective (Zeiss). The filter combinations used were as follows: Fura-2: 340/26 (excitation), 380/10 (excitation), 535/40 (emission), 455 (dichroic); YFP FRET: 430/24 (excitation), 535/25 (emission), 455 (dichroic); CFP: 430/24 (excitation), 470/24 (emission), 455 (dichroic); YFP: 495/10 (excitation), 535/25 (emission),

515 (dichroic); GFP: 480/20 (excitation), 510/20 (emission), 495 (dichroic); mCherry: 577/20 (excitation), 630/60 (emission), 595 (dichroic).

Calcium imaging

MEF DKO cells reconstituted with PS1 (WT or mutant) were identified by mCherry or GFP fluorescence. In general we selected cells expressing a similar amount of mCherry (or GFP) fluorescence as this would indicate a similar amount of PS1 expression. Over the range of intensities, we did not see a correlation between expression level (as assessed by mCherry or GFP) and calcium phenotypes.

For Fura-2 studies, cells were incubated at room temperature with 5μM Fura-2-AM and 3μM Pluronic® F-127 (Invitrogen) for 45 minutes followed by a 15 minute incubation in 1 mL HHBSS to allow for cleavage of the AM-ester. Cells were placed in fresh HHBSS (1 mL) before imaging. Calcium release from the ER was induced by 5 μM ATP (Sigma). At the end of each experiment, Fura-2 was calibrated by adding 5 mM EGTA and 5 μM ionomycin to obtain an R_{min} before adding 5 μM ionomycin and 10 mM Ca^{2+} to obtain an R_{max}. Concentrations of Ca^{2+} were determined using the formula $[Ca^{2+}] = K_d[(R_{max}-R)/(R-R_{min})]*S_f/S_b$, where K_d is 220nM, R is the ratio of emission intensity at 535 nm upon excitation at 340 nm divided by the emission intensity at 535 nm upon excitation at 380 nm at each time point, S_f is the emission intensity upon excitation at 380nm in the Ca^{2+}-depleted state, and S_b is the emission intensity upon excitation at 380nm in the maximum Ca^{2+} state [21]. R_{max}, R_{min}, S_f, and S_b were determined individually for each cell. All images were background corrected prior to determining the ratio (R).

For studies using D1ER, cells were transfected 48 h prior to imaging. Cells were either treated with 4 μM thapsigargin or 3 μM 2,5-Di-(*t*-butyl)-1,4-hydroquinone (tBHQ) (Calbiochem) in Ca^{2+}-free HHBSS. These concentrations were chosen to obtain robust release of Ca^{2+} from the ER. For SERCA activity experiments, cells were washed in Ca^{2+}-free HHBSS to remove tBHQ before adding Ca^{2+}. The D1ER sensor was calibrated in cells at the end of each experiment using 5 μM ionomycin and 5 mM EGTA to obtain an R_{min}. The FRET ratio (R) is proportional to the amount of Ca^{2+} and is defined as the emission intensity in the FRET channel (CFP excitation, YFP emission) divided by the emission intensity in the CFP channel (CFP excitation, CFP emission). We attempted to find the maximum ratio of the sensor (R_{max}) when saturated with Ca^{2+} using established methods [22]; however, the cells did not survive the calibration procedure. Because R_{max} is necessary to convert the FRET ratio into a $[Ca^{2+}]$, we instead report the ΔR ($R- R_{min}$), which is proportional to $[Ca^{2+}]$ and allows comparison of the relative amount of Ca^{2+} in cells expressing the various PS1 mutants. We find this is more accurate than simply comparing R because it incorporates the calibration for R_{min} in each individual cell. All intensities were background corrected before ratioing.

Analysis of calcium spiking

To quantify the period between individual Ca^{2+} spikes, the broad Ca^{2+} decay curves were fit to a single exponential, which was then subtracted from the response curve. The obtained residuals correspond to the oscillatory component of the signal (Supplementary Figure S3). The spiking period was then calculated using the peak finding routine in IGOR Pro (Wavemetrics Inc.). The number of spikes in each time period was normalized to the total number of spikes to obtain the percent of spikes that fell in each time period. The total number of spikes for each cell condition was as follows: DKO 211 spikes (25 cells from 3 exps); WT 274 spikes (34 cells from 3 exps); DKO + WT 41 spikes (5 cells from 3 exps); DKO + L166P 60 spikes (5 cells from 4 exps); DKO + M233V 29 spikes (4 cells from 2 exps); DKO + A409T 76 spikes (6 cells from 2 exps). Because images were acquired every

3 sec oscillations with a period faster than 6 sec could not be measured due to the Nyquist criterion.

Statistical Analysis

Statistical analysis on data was performed using Kaleidagraph 4.0 (Synergy Software). Data are represented as the mean ± SEM. Differences between the means were compared using an ANOVA with Student-Newman-Keuls post-hoc test to determine statistical significance ($P < 0.05$).

Supplementary Material

Refer to Web version on PubMed Central for supplementary material.

Acknowledgments

We would like to thank the following sources for financial support: University of Colorado Signaling and Cell Cycle Regulation Training Grant (NIH T32 GM08759), NIH GM084027 to A. E. P., and the University of Colorado.

Abbreviations

APP	amyloid precursor protein
fAD	familial Alzheimer's disease
FRET	Fluorescence Resonance Energy Transfer
R	FRET ratio
IP_3	Inositol-1,4,5-trisphosphate
IP_3R	Inositol-1,4,5-trisphosphate receptor
PS1	Presenilin-1
PS2	presenilin-2
MEF	mouse embryonic fibroblast
DKO	presenilin-1 and presenilin-2 double knock out
PM	Plasma Membrane
SERCA	Sarco-Endoplasmic Reticulum ATPase

References

1. Tu H, Nelson O, Bezprozvanny A, Wang Z, Lee SF, Hao YH, Serneels L, De Strooper B, Yu G, Bezprozvanny I. Cell. 2006; 126:981–993. [PubMed: 16959576]
2. Green KN, Demuro A, Akbari Y, Hitt BD, Smith IF, Parker I, LaFerla FM. J Cell Biol. 2008; 181:1107–1116. [PubMed: 18591429]
3. Cheung KH, Shineman D, Muller M, Cardenas C, Mei L, Yang J, Tomita T, Iwatsubo T, Lee VM, Foskett JK. Neuron. 2008; 58:871–883. [PubMed: 18579078]
4. Smith IF, Hitt B, Green KN, Oddo S, LaFerla FM. J Neurochem. 2005; 94:1711–1718. [PubMed: 16156741]
5. Chan SL, Mayne M, Holden CP, Geiger JD, Mattson MP. J Biol Chem. 2000; 275:18195–18200. [PubMed: 10764737]
6. Sherrington R, Rogaev EI, Liang Y, Rogaeva EA, Levesque G, Ikeda M, Chi H, Lin C, Li G, Holman K, et al. Nature. 1995; 375:754–760. [PubMed: 7596406]

7. Duff K, Eckman C, Zehr C, Yu X, Prada CM, Perez-tur J, Hutton M, Buee L, Harigaya Y, Yager D, Morgan D, Gordon MN, Holcomb L, Refolo L, Zenk B, Hardy J, Younkin S. Nature. 1996; 383:710–713. [PubMed: 8878479]
8. Marx J. Science. 2007; 318:384–385. [PubMed: 17947560]
9. LaFerla FM. Nat Rev Neurosci. 2002; 3:862–872. [PubMed: 12415294]
10. Bezprozvanny I, Mattson MP. Trends Neurosci. 2008; 31:454–463. [PubMed: 18675468]
11. Stutzmann GE, Caccamo A, LaFerla FM, Parker I. J Neurosci. 2004; 24:508–513. [PubMed: 14724250]
12. Nelson O, Tu H, Lei T, Bentahir M, de Strooper B, Bezprozvanny I. J Clin Invest. 2007; 117:1230–1239. [PubMed: 17431506]
13. Zatti G, Burgo A, Giacomello M, Barbiero L, Ghidoni R, Sinigaglia G, Florean C, Bagnoli S, Binetti G, Sorbi S, Pizzo P, Fasolato C. Cell Calcium. 2006; 39:539–550. [PubMed: 16620965]
14. Leissring MA, Akbari Y, Fanger CM, Cahalan MD, Mattson MP, LaFerla FM. J Cell Biol. 2000; 149:793–798. [PubMed: 10811821]
15. Leissring MA, Paul BA, Parker I, Cotman CW, LaFerla FM. J Neurochem. 1999; 72:1061–1068. [PubMed: 10037477]
16. Palmer AE, Jin C, Reed JC, Tsien RY. Proc Natl Acad Sci U S A. 2004; 101:17404–17409. [PubMed: 15585581]
17. Herreman A, Hartmann D, Annaert W, Saftig P, Craessaerts K, Serneels L, Umans L, Schrijvers V, Checler F, Vanderstichele H, Baekelandt V, Dressel R, Cupers P, Huylebroeck D, Zwijsen A, Van Leuven F, De Strooper B. Proc Natl Acad Sci U S A. 1999; 96:11872–11877. [PubMed: 10518543]
18. Herreman A, Van Gassen G, Bentahir M, Nyabi O, Craessaerts K, Mueller U, Annaert W, De Strooper B. J Cell Sci. 2003; 116:1127–1136. [PubMed: 12584255]
19. Berridge MJ, Bootman MD, Roderick HL. Nat Rev Mol Cell Biol. 2003; 4:517–529. [PubMed: 12838335]
20. Kasri NN, Kocks SL, Verbert L, Hebert SS, Callewaert G, Parys JB, Missiaen L, De Smedt H. Cell Calcium. 2006; 40:41–51. [PubMed: 16675011]
21. Grynkiewicz G, Poenie M, Tsien RY. J Biol Chem. 1985; 260:3440–3450. [PubMed: 3838314]
22. Palmer AE, Tsien RY. Nat Protoc. 2006; 1:1057–1065. [PubMed: 17406387]

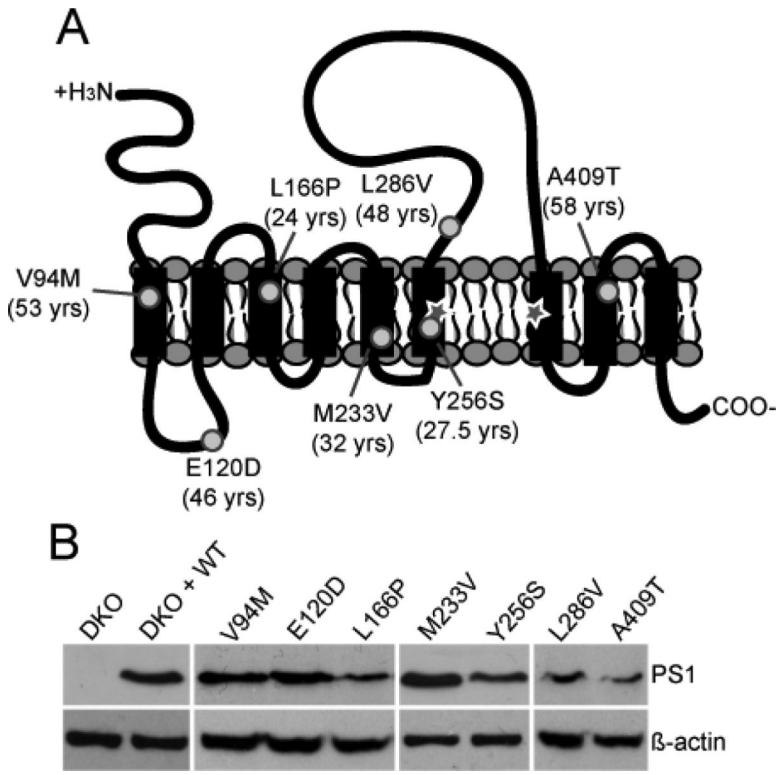

Figure 1.

Verification of PS1 in cells. (A) Schematic of PS1 showing proposed membrane topology and relative locations of the mutations (circles) chosen for this study. Critical aspartates are denoted by a star. Average age at onset is indicated in parentheses. (B) Western blot showing relative expression levels of the PS1 variants upon transient transfection into DKO cells.

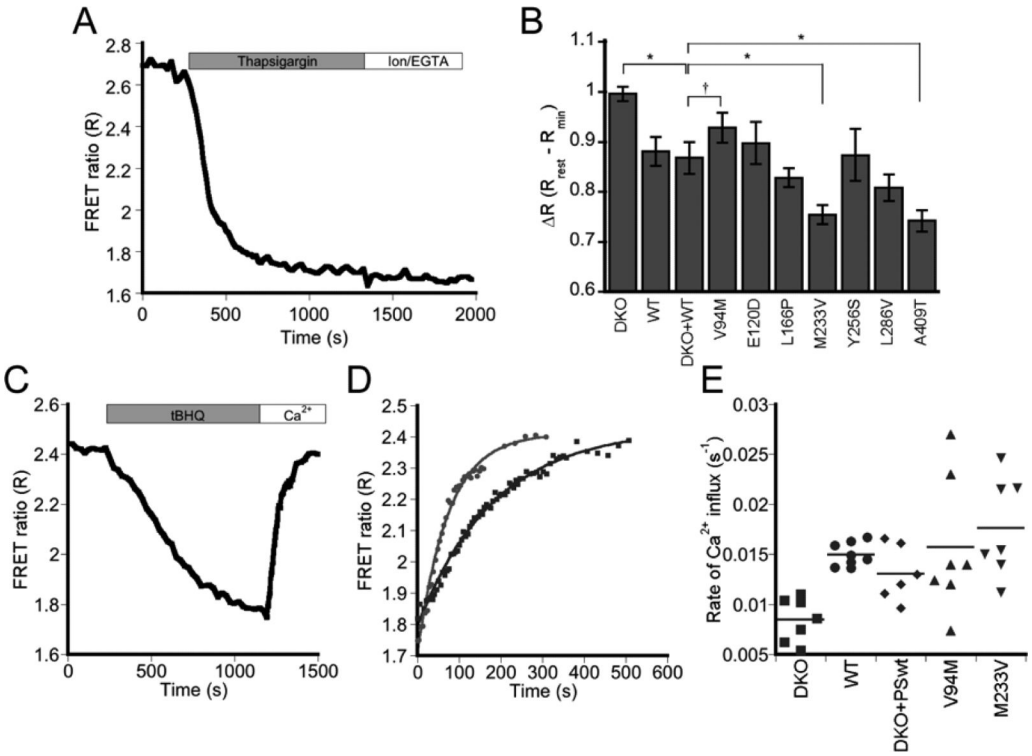

Figure 2.

Impact of PS1 on Ca^{2+} within the ER. (A) Representative experiment measuring ER Ca^{2+} load using the D1ER Ca^{2+} sensor. MEF cells transfected with the PS1 mutants were treated with thapsigargin in the absence of extracellular Ca^{2+} before calibrating the sensor with EGTA and ionomycin to obtain R_{min}. (B) Bar graph showing ΔR at rest in the ER. Error bars indicate SEM. Asterisk: $P < 0.05$, ANOVA with Student-Newman-Keuls post-hoc test. Dagger: V94M appears to have more Ca^{2+} in the ER compared to control, though the difference is not statistically significant.WT: n = 17 (5 exps); DKO: n = 24 (9 exps); DKO + WT: n = 8 (6 exps), E120D: n = 8 (6 exps); V94M: n = 11 (7 exps); L166Pn = 13 (6 exps); M233V: n = 9 (4 exps); Y256S: n = 7 (3 exps); L286V: n = 13 (5 exps); A409T: n = 9 (5 exps). (C) Representative experiment examining the refilling of ER Ca^{2+} stores using D1ER. Cells were treated with tBHQ before adding excess Ca^{2+} to reload the ER. (D) Rates of ER refilling in WT (gray circles) and DKO (black squares). Data are fit to an exponential rise, $A(t) = A_0(1 - e^{-kt})$. (E) Plot of Ca^{2+} influx rate constants (k). Only DKO shows significant difference from WT ($P < 0.015$, ANOVA with Student-Newman-Keuls post-hoc test). Each point represents the k from an individual experiment and the horizontal line marks the mean k value for each data set. WT: n = 8 from 3 exps; DKO: n = 7 from 5 exps; DKO + WT: n = 6 from 4 exps; V94M: n = 7 from 4 exps; M233V: n = 7 from 3 exps.

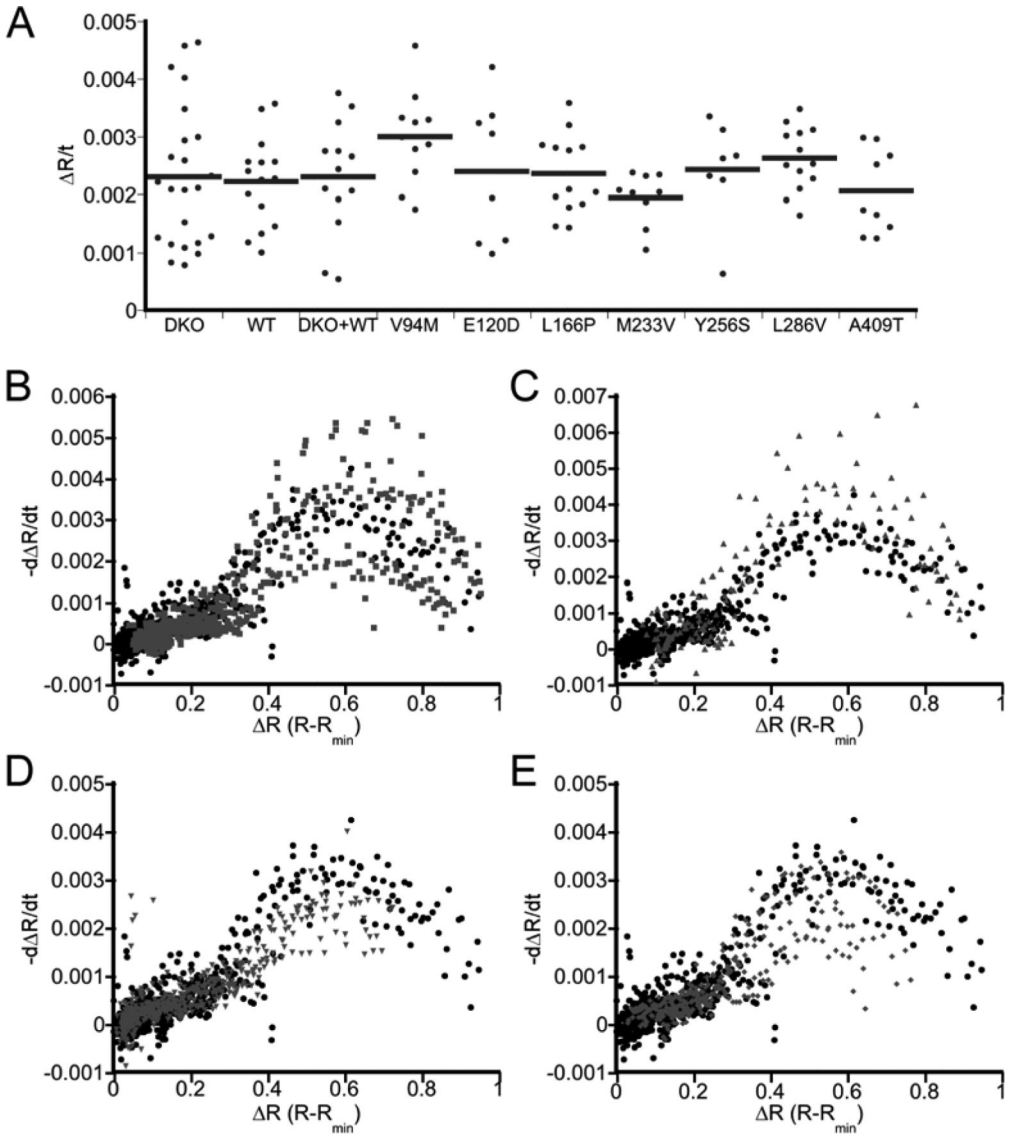

Figure 3.

Effect of PS1 on ER Ca^{2+} leak rates. (A) Initial Ca^{2+} leak rate, defined as the change in ratio per unit time (ΔR/t). Rates were determined from the first 150 s after treatment of cells with 4 μM thapsigargin using a linear fit. (B – E) Comparison of Ca^{2+} leak rate as a function of Ca^{2+} concentration, reported as the rate of change of the ratio (dΔR/dt) as a function of the ΔR for WT (black) versus DKO (B), V94M (C), M233V (D) and A409T (E) in gray.

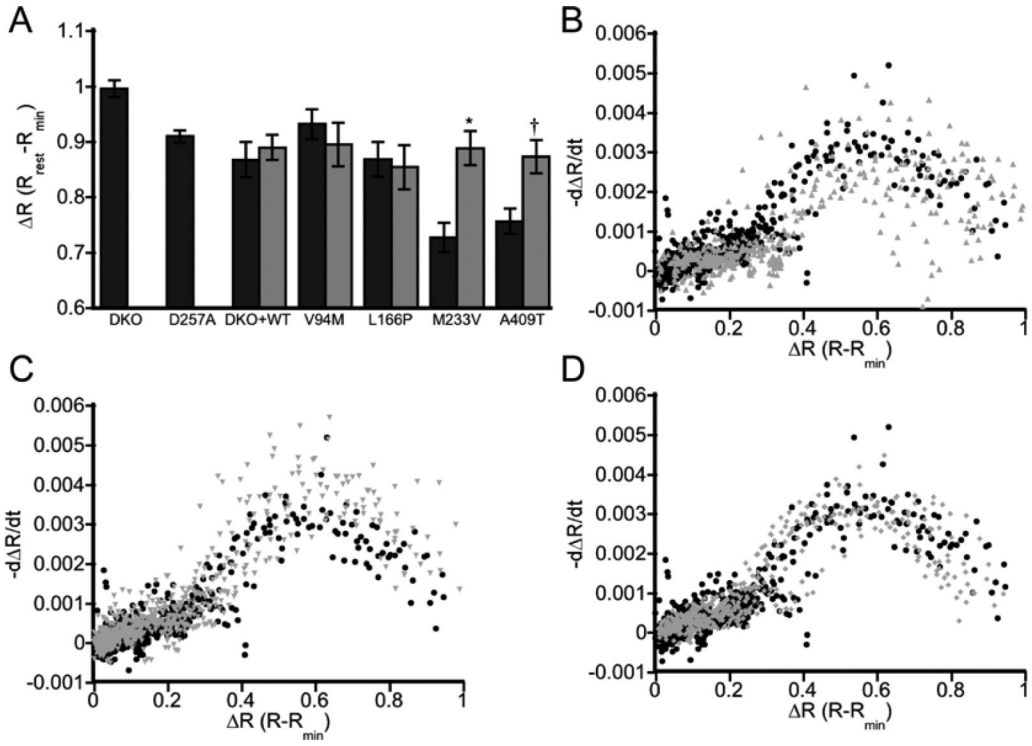

Figure 4.

Gamma-secretase activity affects ER Ca^{2+} levels. (A) Bar graph depicting ΔR at rest in the ER for cells with (light gray) and without (dark gray) 24 h treatment with the gamma-secretase inhibitor DAPT. Error bars indicate SEM. Asterisk: $P < 0.0005$, unpaired t-test; Dagger: $P < 0.005$, unpaired t-test. DKO + WT: n = 6 (3 exps); V94M: n = 14 (2 exps); L166P: n = 13 (4 exps); M233V: n = 23 (4 exps); A409T: n = 16 (4 exps). (B – D) Comparison of the ER Ca^{2+} leak rate as a function of relative Ca^{2+} concentration. Leak rates are reported as a rate of change in the normalized ratio (ΔR) versus ΔR for V94M (B), M233V (C) and A409T (D). Graphs depict mutant leak rates (gray) compared to leaks rates in WT not treated with DAPT (black)

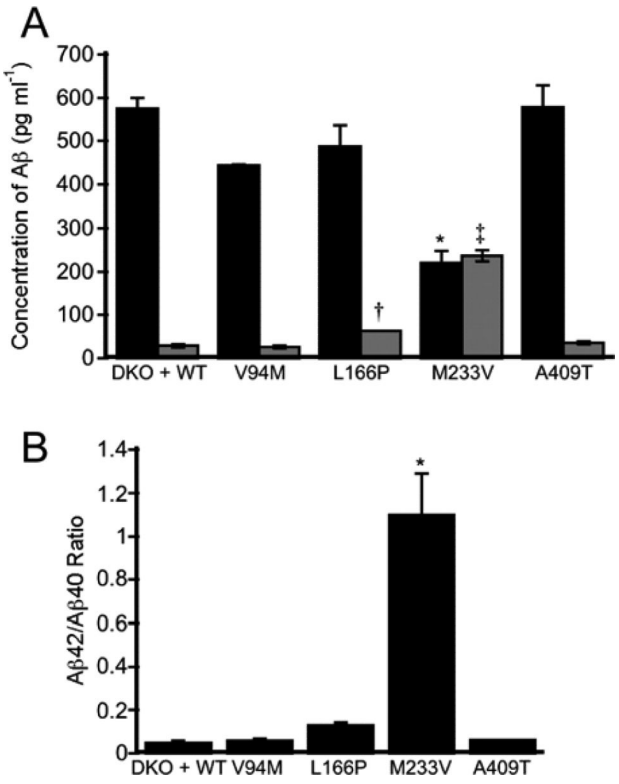

Figure 5.

Examination of gamma-secretase mediated cleavage of APP. (A) Relative amounts of Aβ40 (dark gray) and Aβ42 (light gray) in cells expressing a subset of the PS1 mutants. Both L166P and M233V led to an increase in Aβ42 levels. M233V also led to a significant decrease in Aβ40 levels. Asterisk: $P < 0.005$; Dagger: $P < 0.05$; Double dagger: $P < 0.0001$. (B) Relative ratios of Aβ42/40 for a subset of the PS1 mutants. Asterisk: $P < 0.002$. All statistics were calculated using an ANOVA with Student-Newman-Keuls post-hoc test. Error bars indicate SEM.

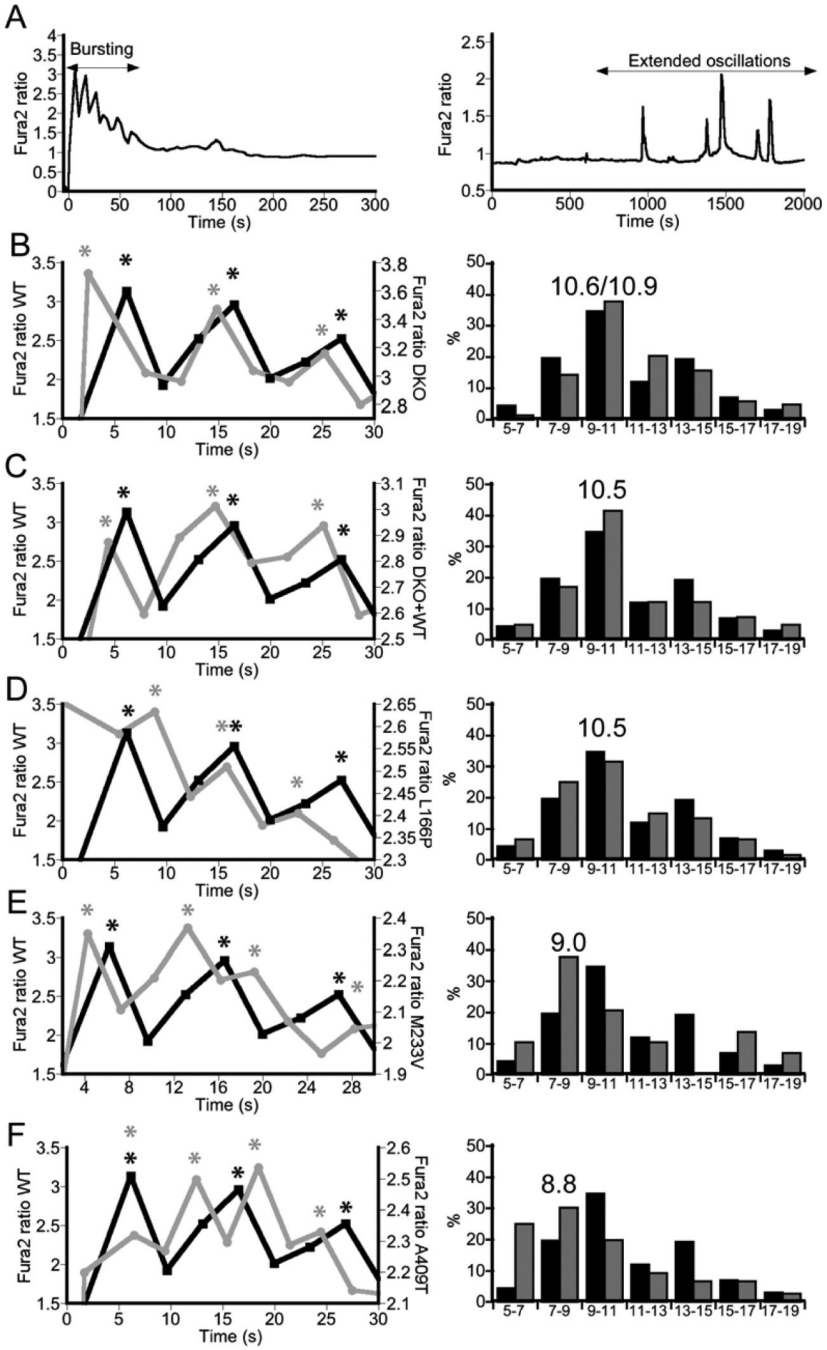

Figure 6.

Effect of mutations in PS1 on kinetics of ER Ca^{2+} release. (A) Cells exhibited either a burst in Ca^{2+} from the ER (left) or, less frequently, irregular extended Ca^{2+} oscillations (right) in response to ATP. Bursting activity was examined to compare mutations in these studies. (B – F) Representative traces of Ca^{2+} bursts (left) compare differences between WT (black) and transfected DKO (gray) in initial release of Ca^{2+} from the ER. Peaks of each spike are indicated by an asterisk. Histograms (right) show the distribution of Ca^{2+} spike periods compared to WT (black; n = 274, 34 cells, 3 exps) for (B) DKO (n = 211, 25 cells, 3 exps), (C) DKO + WT (n = 41, 5 cells, 3 exps), (D) DKO + L166P (n = 60, 5 cells, 4 exps), (E)

DKO + M233V (n = 29, 4cells, 2 exps) and (F) DKO + A409T (n = 76, 6 cells, 2 exps) after treatment with 5 μM ATP. The median period for spiking is given above the histogram.